Electrochemical deposition of p-type FeS_2 thin films absorber layer for photovoltaic cell

P. Prabukanthan[1*], R. Lakshmi[1], T. Rajesh Kumar[1], S.Thamaraiselvi[1], G. Harichandran[2]

[1]*Materials Chemistry Lab, Department of Chemistry, Muthurangam Government Arts College, Vellore632002, India*
[2]*Department of Polymer Science, University of Madras, Chennai600025, India*

[*]Corresponding author: Tel: +(91) 0416-2262068; E-mail: pprabukanthan76@hotmail.com

Received: 30 March 2016, Revised: 17 September 2017 2016 and Accepted: 18 April 2017

DOI: 10.5185/amp.2017/811
www.vbripress.com/amp

Abstract

Electrochemical deposition (ECD) of FeS_2 thin films from aqueous solution contains $FeSO_4$, $Na_2S_2O_3.5H_2O$ and H_2SO_4. ECDs were performed at different bath temperatures (30, 40, 50, 60 and 70°C) with constant pH (~2). FESEM images shows that the grains are as deposited films with stoichiometric iron pyrite thin films were successfully formed at 50, 60 and 70°C and S/Fe ratio in as-deposited films were ~2. GAXRD studies of as-deposited at 30 and 40°C FeS_2 thin films shows a minor phase of orthorhombic marcasite and major cubic pyrite phase observed. As-deposited thin films at 50, 60 and 70°C brings about the formation of FeS_2 with single crystalline cubic phases with a strong (111) preferred orientation and without any contribution of marcasite phase. When the bath temperature was increased, as-deposited thin films of crystalline size, thickness and roughness value increased due to rate of formation FeS_2 increased. Raman spectra of the FeS_2 thin films presented characteristic peaks of S-S active mode at 377 cm^{-1}. The optical spectra of the as-deposited FeS_2 thin films with different bath temperatures showed a clear absorption edge band gap of these films from 0.86 to 0.96 eV. As-deposited FeS_2 thin films at different bath temperatures show p-type conductivity.

Keywords: Iron pyrite, electrochemical deposition, structural properties, optical properties, electrical properties.

Introduction

Iron pyrite (cubic-FeS_2) has been of continuous interest since the 1970s due to its abundance, absorber layers of solar cells due to excellent hole mobility, photo-absorption characteristics and with suitable energy band gap [**1-3**]. The iron pyrite layer with the 10 nm thickness can generally produce the sunlight absorption higher than 90%. Therefore, the pyrite can be utilized as thin film materials in the photoelectrical conversion system. The low-cost preparation methods are favourably considered. Most of them are based on the sulphuration of some precursors Fe [**4-5**], Fe oxides [**6**] and Fe sulphides [**7-8**]. By solution methods are used to make pyrite thin films include spray pyrolysis [**9-12**], electrochemical deposition (ECD) [**13-17**], chemical bath deposition (CBD) [**18-19**], electrophoretic deposition (EPD) [**20**] and sol gel chemistry [**21−22**]. The strategy adopted for the deposition of iron oxide or iron sulphide films (often amorphous) and anneal the film in sulphur gas at elevated temperatures (350−600 °C) to produce polycrystalline pyrite. Despite of this, the conversion efficiency of FeS_2 solar cells has not exceeded to 3% [**1**]. The reason for the low conversion efficiency can be attributed to phase impurity [**22**]. Generally FeS_2 can crystallize not only into a cubic pyrite structure, but also into a metastable orthorhombic marcasite structure that is detrimental to photovoltaic applications with its low bandgap (E_g = 0.34 eV) and polymorphs differing in their chemical structure by linking of Fe-centered octahedral. Pyrite devices display some high quantum efficiencies but suffer from low open- circuit voltages (V_{OC} = 200 mV, which has been attributed to surface defects [**1**]. The photovoltaic properties of pyrite can be improved by stronger interfacial interaction between donor-accepter layers [**23**]. Although, the pyrite and marcasite phase compounds are diamagnetic in nature [**24**]. Therefore, new and improved techniques are needed to resolve these problems. Moreover, a simple method is developed for the preparation of crystalline pyrite thin films with large area by using simple ECD equipment. ECDs presents an interesting a potentially fast deposition rates over large areas and this low cost thin film deposition method with many advantages: the possibility of controlling film properties thickness through the electrochemical variables, substrates of variable sizes and shapes can be used under low temperatures. In this deposition process can be controlled and the reactions are involved as closer to equilibrium than in many gas phase methods. In this present work, iron pyrite (FeS_2) thin films were conveniently prepared by ECD method. As-deposited FeS_2 thin films were characterized by glancing angle X-ray diffraction (GAXRD), Raman spectroscopy, field emission scanning electron microscopy (FESEM), energy dispersive X-ray analysis (EDAX), UV-visible spectra and electrical (Hall Effect) measurements.

Experimental

Chemical and materials

Ferrous sulphate ($FeSO_4$) (3N) and sodium thiosulphate ($Na_2S_2O_3.5H_2O$) (3N) were procured from Sigma-Aldrich (USA). Sulpuric acid (H_2SO_4) has purchased from Spectrochem (India). All the chemicals used without further purification for the preparation of solutions. Double distilled water was used to prepare all the solutions and to rinse the electrodes.

Deposition of iron pyrite (FeS_2) thin films by electrochemical deposition (ECD)

FeS_2 thin films were ECD on ITO coated glass substrates (resistance of ~10 Ω/sq, thickness of the conducting layer being 180 nm and transparency around 83% at 550 nm) at different bath temperatures (30, 40, 50, 60 and 70°C) using a simple conventional three electrode system (CH Instruments 604E, USA). To start with the ITO coated glass substrates were cleaned in an ultrasonic bath with ethanol solvent to remove any adhering impurities and then washed with double distilled water. In a three-electrode system a ITO coated glass substrate as the working electrode, saturated calomel [Ag^+/AgCl/KCl] electrode (SCE) as the reference electrode and Pt wire as the counter electrode. Linear sweep voltammetry (LSV) technique was used to ECD of the FeS_2 thin films. For ECD experiments the deposition solution was prepared by mixing 10 ml of 0.05 $moldm^{-3}$ $FeSO_4$, 20 ml of 0.152 $moldm^{-3}Na_2S_2O_3.5H_2O$ and 60 ml double distilled water and it was stirred for few minutes to make homogenous solution. ECD bath solution pH (~2) was adjusted by adding sulphuric acid and the ECD were performed at constant potential deposition (-850 mV) and the fixed duration of 600 seconds. The deposited FeS_2 thin films were washed thoroughly with double distilled water followed by ethanol and kept for the further characterisation of the thin films.

Characterization of as-deposited FeS_2 thin films

Structural elucidation of the as-deposited FeS_2 thin films at different temperatures were carried out by GAXRD studies using a Bruker AXS Diffractometer Plus/D8 Advanced Spectrometer with Cu Kα (λ = 1.5405 Å) radiation with a scan speed of 1˚ per min and with the increment of 0.02˚. The glancing angle was fixed at 2˚. Raman spectra of as-deposited FeS_2 thin films at different temperatures were recorded at room temperature. The excitation source was an argon ion laser beam of 30 mW (λ=488nm) power with vertical polarization focused to a spot size of 50 μm onto the sample. The scattered light was collected in the backscattering geometry using a camera lens (Nikkon; focal length, 5 cm; *f*/1.2). The collected light was dispersed in a double grating monochromator, SPEX model 14018, and detected using thermoelectrically cooled photomultiplier tube model ITT-FW 130. The resolution obtained was 5 cm^{-1}. The surface morphology of the as-deposited FeS_2 thin films at different temperatures were examined by a field emission scanning electron microscope (FESEM), Hitachi S-4300SE, operating at an accelerating voltage of 10 kV. The chemical compositions of the as-deposited FeS_2 thin films at different temperatures were studied using EDAX, INCA 200 system connected to a SEM operating at an accelerating voltage of 20 kV. The optical transmission spectra of the as-deposited FeS_2 thin films at different temperatures were recorded using Shimadzu UV–visible NIR spectrometer in the range 200–1800 nm. Electrical measurements on the as-deposited FeS_2 thin films at different temperatures were measured by using Hall-effect measurement apparatus with van der Pauw configuration with gold (Au) contacts and the indium soldered platinum wires to the contact plates were used. I-V measurement was also performed by Keithley 4200 I-V unit.

Results and discussion

The iron pyrite (FeS_2) thin films were deposited by ECD method and the thin films were uniform and well adhered onto the ITO substrate.On the basis of aqueous chemistry of thiosulphate and Fe(II) in an acidic medium, one could expect the formation of FeS_2 by this deposition.The dissociation of thiosulphate in water gives rise to S^{2-} and elemental S, which can further combine and give the disulfide (S_2^{2-}) ions:

$$2S_2O_3^{2-} + 2H_2O \Leftrightarrow 2SHO_4^{2-} + S + H_2S + 2H^+ \Leftrightarrow 2S^{2-} + 4H_2O \quad (1)$$

Fe(II) and disulfide ions condense with electrical force in the solution or on the substrate to the deposition of FeS_2.

$$Fe^{2+} + S_2^{2-} \Longleftrightarrow FeS_2 \quad (2)$$

In the ECD, the Fe^{2+} ions are generated and attract towards the cathode. Overall the cathodic reaction may be cited as,

$$Fe^{2+} + S_2O_3^{2-} + 6H^+ + 6e^- \Longleftrightarrow FeS_2 + 3H_2O \quad (3)$$

The as-deposited FeS_2 thin film at different bath temperatures, thickness and roughness values were evaluated from the profilometer and the data were presented in **Table 1**. Thickness and roughness of as-deposited thin films increases with increase in the bath temperature. It's due to consequently the nucleation of iron containing sulphide phase can occur faster.

Table 1. Thickness, roughness, composition, lattice parameters, FWHM, crystallite size, micro strain, dislocation density, number of crystallites per unit area of as-deposited FeS_2 thin films at different bath temperatures.

Deposition temperature (°C)	Thickness (nm)	Roughness (nm)	Composition (atomic percentage)		Lattice parameters (nm)	FWHM of GAXRD peak (111) (deg.)	Crystallite size (nm)	Micro strain ($x10^{-3}$)	Dislocation density ($x10^{14}$ lines/m^2)	Number of crystallites per unit area ($x10^{16}m^{-2}$)
			Fe (%)	S (%)						
30	620	17.6	34.42	65.58	0.5448	0.02567	46	5.44	6.3	3.5
40	780	20.4	34.21	65.79	0.5478	0.02743	52	5.22	6.1	3.8
50	830	23.4	33.34	66.66	0.5381	0.02847	53	5.01	5.9	3.9
60	840	24.1	34.43	66.57	0.5408	0.02893	60	4.87	5.4	4.3
70	870	24.9	33.40	66.60	0.5418	0.02921	69	4.23	5.1	4.9

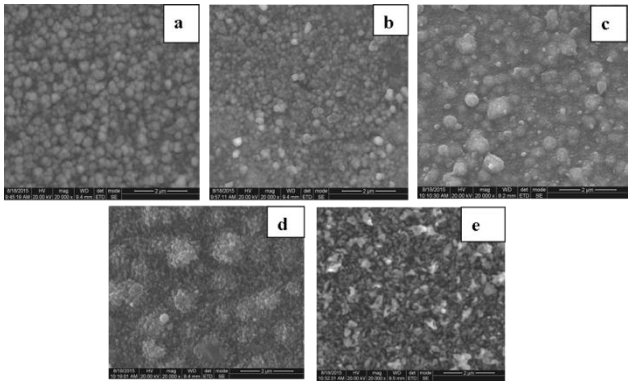

Fig. 1. (a-e) FESEM of as-deposited FeS_2 thin films at different bath temperatures (a) 30 °C, (b) 40 °C, (c) 50 °C, (d) 60 °C and (e) 70°C.

The morphologies of the FeS_2 thin films were observed in the field emission scanning electron microscope (FESEM) images. **Fig. 1(a-e)** shows the FESEM micrographs of the surface of the as-deposited iron pyrite at different bath temperatures and the morphologies shows that uniformly covered films with a free of cracks all over the surface of the as-deposited films. Further, a significant grain growth results also shows that without porous and cracks free types of morphology.

Chemical compositions of the films were analyzed from EDAX spectral data of different regions of the films recorded with an incident electron beam of 20 keV. **Table 1** show that the compositions, arrived at by EDAX of the as-deposited iron pyrite thin films under different bath temperatures. It is found that the relative content of Fe slightly higher with respect to relative content of S slightly lower in as-deposited at bath temperature 30 and 40°C. Using the relative proportions expressed in an atomic percent (at %), the S/Fe ratio was determined as 1.90 and 1.92 in as-deposited at bath temperature 30 and 40°C. Hence its films were sulphur deficiency. The S/Fe ratio 1.99 in as-deposited at bath temperature 50, 60 and 70°C, respectively.

Glancing angle X-ray diffraction (GAXRD) patterns of as-deposited FeS_2 thin films at different bath temperature of 30, 40, 50, 60 and 70°C are shown in **Fig. 2(a-e)** and where Bragg lines are indexed of the GAXRD spectrum. From the GAXRD, it was possible to identify the crystalline phases that constitute the samples as pyrite, although at low bath temperature shows some other peaks appear which could be attributed to marcasite phase. The GAXRD patterns of different bath temperatures as-deposited FeS_2 thin films have indicated the strong reflections from the cubic pyrite (FeS_2) phase of (111) plane. **Fig. 2(a-b)** presents addition reflections originating from (011) and (020) planes of orthorhombic marcasite (FeS_2) phase present in as-deposited FeS_2 thin films at bath temperatures of 30 and 40°C. However, the deposition (formation) of marcasite phase has iron rich (discussion in composition part). As-deposited at bath temperature 50, 60 and 70°C FeS_2 thin films corresponding to stoichiometric composition and consists of a single crystalline pyrite phase without any contributions from other phases (**Fig. 2(c-e)**. The GAXRD peaks can be indexed to the (111), (200), (220) and (222) planes of cubic phases of FeS_2, respectively. From thermodynamic data, the pyrite Gibbs energy of formation is more negative than that of marcasite at any temperature. This fact led us to conclude that formation of marcasite is not due to thermodynamic stability but to kinetic reasons. The observed peaks 'd' spacing values are in good agreement with standard JCPDS card no 79-0617 for cubic pyrite (FeS_2). From (hkl) planes, the lattice constant (a) were evaluated using the relation $[a = d (h^2 + k^2 + l^2)^{1/2}]$, where d is inter-planar spacing of the atomic planes. The calculated d-spacing values have been used to determine the lattice constant and these values are presented in **Table 1**. The lattice constant (a) was increased slightly with lower bath temperature (30 and 40°C). But higher bath temperature doesn't affect in the lattice constant. As-deposited thin films above 40°C it may be high densely packed in crystalline lattice. The low value of lattice constant is due to that the lattice could be contracted. **Table 1** lists the full width at half maximum (FWHM) values of (111) diffraction peak of the FeS_2 thin films. The FWHM of the (111) peak of the FeS_2 thin films obtained from bath temperatures are higher than that of lower bath temperature. The reason may be smaller strain occur in the as-deposited thin films obtained from higher bath temperature.

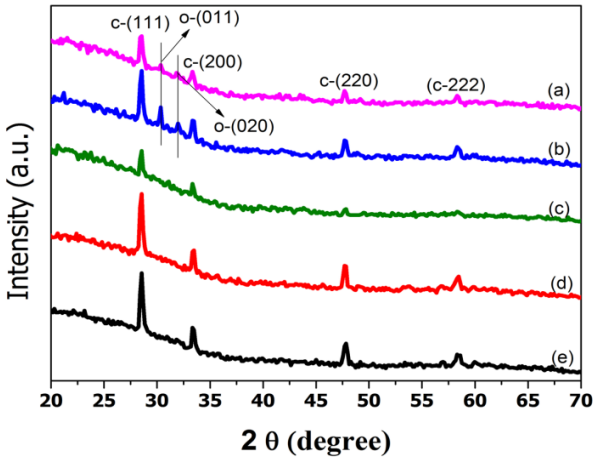

Fig. 2. (a-e) GAXRD spectra of as-deposited FeS_2 thin films at different bath temperatures (a) 30 °C, (b) 40 °C, (c)50 °C, (d) 60 °C and (e) 70°C.

As the deposited thin films have regular shape and size therefore the average crystallite size (D) was evaluated from the FWHM of the (111) diffraction peak using Scherer's equation [$D = 0.9\ \lambda/\beta\ \cos\theta$], where β is the FWHM of the diffraction line in radians and λ is the X-ray wavelength [**18**]. The calculated average crystallite sizes were found to be in the range of 46-69 nm and these are listed in **Table 1**. For photovoltaic applications, the greater crystallite size and the lower grain boundary recombination to get the higher the current output [**5**]. The micro strain (ε), dislocation density (δ) and number of crystallites per unit area (N) were calculated using the following relations (equations (6), (7) and (8)) and their values are given in **Table 2**.

$$\text{Micro strain } (\varepsilon) = \beta \cos\theta/4 \quad (4)$$

$$\text{Dislocation density } (\delta) = 15\varepsilon/aD \quad (5)$$

$$\text{Number of crystallites } (N) = t/D^3 \quad (6)$$

where, θ, the Bragg's angle and t, thickness of the film. The decreases of ε and δ values with increases in the bath temperature may be due to crystalline lattice densely packed with to its grain boundary which leads to increases in the concentration of lattice perfections.

Raman spectra of as-deposited iron pyrite thin films are shown in **Fig. 3**. Raman spectroscopy is more sensitive than XRD to marcasite impurities near the film surface [**22**]. Raman spectra of the as-deposited at lower bath temperatures 30 and 40°C shows that Raman bands for both orthorhombic marcasite (at 322 cm^{-1}) and cubic pyrite (at 377 cm^{-1}) [orthorhombic marcasite is the common polymorph of FeS_2], which are the characteristic active modes for pyrite corresponding to the S_2libration (E_g), S-S in phase stretch (A_g) and coupled libration and stretch (T_g) modes, respectively [**25**]. The dominant mode in the iron pyrite spectra is E_g vibration mode at 377 cm^{-1}. This peak is the characteristic active mode for pyrite corresponding to the vibration of the S atom perpendicular to the dumb-bell axes. In the case of Raman spectra of the as-deposited at higher bath temperatures 50, 60 and 70°C did not show the orthorhombic marcasite at 322 cm^{-1}. However, T_g vibrational band 377 cm^{-1} and 426 cm^{-1} are present.

Fig. 4 shows $(\alpha h\nu)^2$ and hν of as-deposited iron pyrite at different bath temperature. The spectra of as-deposited iron pyrite thin films are shows that a clear absorption edge and indicates that the films have good crystalline nature with uniform optical properties [Eg = 0.86-0.96 eV] due to indirect transition in the pyrite film. A similar result was observed in the literature of 0.95 eV [**21**]. The presence of marcasite minor phase in FeS_2 thin films is generally not to alter the bandgap of the major pyrite phase. As a result bath temperature increases, as-deposited thin films thickness were increased for the films with the thickness above 800 nm the value of Eg increases. Since the specific surface area of the films decreases to weaker the effect of surface factors.

The conductivity type, resistivity, hole concentration and hole mobility wereh measured the as-deposited iron pyrite thin films **(Table 2).** The as-deposited thin films are of p-type conductivity, as indicated by the hot-probe and Hall effect measurements applying van der Pauw method [**26**]. As-deposited iron pyrite at bath temperatures of 30 and 40°C, the resistivity was larger than that of 50, 60 and 70°C, whereas their hole concentration were smaller than the same. This may be attributed to the formation of stoichiometric deviation and more grain boundaries appeared in the films with reduced grain size. It is noted that hole mobility increases with film thickness (bath temperature increases) markedly. According to grain boundary model, the decreased defect concentration in thicker film leads to the lowering of potential barrier at the grain boundaries and it provides more hole carriers. Further, the higher hole mobility and hole concentration are due to the closed stoichiometric composition or disorder of cation and anion vacancies are low.

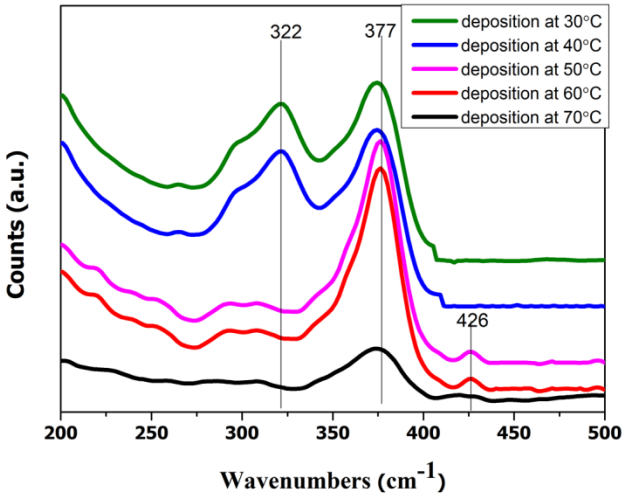

Fig. 3. Raman spectra of as-deposited FeS_2 thin films.

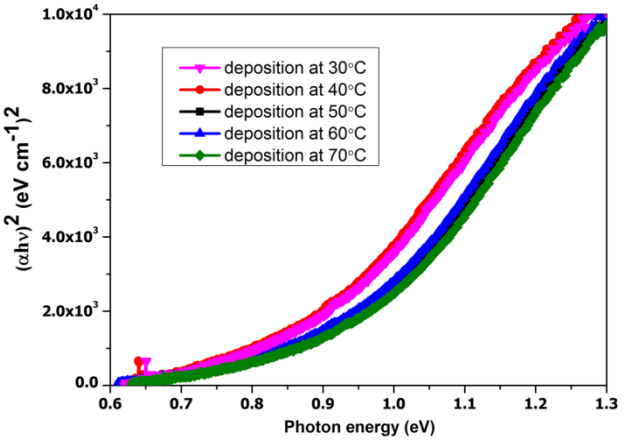

Fig. 4. $(\alpha h\nu)^2$ and hνspectra of as-deposited FeS_2 thin films.

Table 2. Room temperature electrical properties of as-deposited FeS_2 thin films at different temperatures.

Deposition temperature (°C)	Resistivity (Ωcm)	Hole concentration (x 10^{27}) (cm^{-3})	Hole mobility ($cm^2V^{-1}s^{-1}$)
30	8.6	3.5	22.1
40	8.5	3.1	22.7
50	3.4	5.9	34.2
60	3.8	6.2	35.4
70	3.9	6.6	38.3

Two-probe I-V measurement was carried out to study the type of deposited semiconductor film materials (n-type or p-type) Indium doped tin oxide (ITO) on which deposition was carried out on the conducting material. It is used as bottom contact and aluminum dots are taken as the top contact from the upper surface of deposited FeS_2 layer (deposited thin film at 70°C). **Fig. 5** shows that the two-probe I-V plots of FeS_2 thin films which is typical diode characteristics between ITO and FeS_2. ITO being

as a n-type semiconductor, so it may be concluded that the FeS_2 films deposited on ITO substrate is a p-type and the contact of aluminum has showing the ohmic behavior. The ITO being highly conducting and the aluminum contact with it will show linear I-V characteristics. Hence, the ohmic behavior is due to the p-FeS_2/n-ITO junction. So, it can be concluded that the FeS_2 thin films deposited on ITO substrate is a p-type.

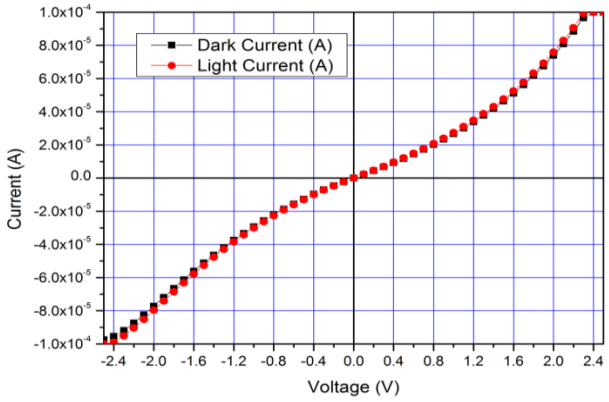

Fig. 5.I-V characteristics for the FeS_2 thin films under dark and light.

Conclusion

Iron pyrite thin films have been deposited on ITO coated glass substrate from an aqueous solution by electrochemical deposition technique at different bath temperatures (30, 40, 50, 60 and 70°C) with constant pH (~2). As-deposited at 30 and 40°C iron pyrite thin films shows marcasite phase were peaks observed and good crystalline phase. As-deposited thin films at 50, 60 and 70°C brings about the formation of FeS_2 with single crystalline cubic iron pyrite phase without any contribution of marcasite phase. The crystallite size, micro strain, dislocation density and number of crystallites per unit were calculated. When bath temperature was increased as well as crystalline size, thickness and roughness were increased, respectively. GAXRD and Raman spectra shows that a pure pyrite phase as-deposited at 50, 60 and 70°C.The band gap was found to be 0.96 eV by optical absorption spectra.

Acknowledgements

One of the authors (P. Prabukanthan) wishes to acknowledge University Grant Commission (UGC), India, for the financial assistance through major research project (MRP) scheme [File No. 43-399/2014(SR)].

References

1. Ennaoui, A.; Fiechter, S.; Pettenkofer, C.; Alonso-Vante, N.; Büker, K.; Bronold, M.; Höpfner, C.; Tributsch, H.; *Sol. Energy Mater. Sol. Cells*, **1993**, 29, 289. **DOI:** 10.1016/0927-0248(93)90095-K
2. Ares, J.R.; Pascual, A.; Ferrer, I.J.; Sánchez, C.; *Thin Solid Films*, **2005**, 480–481, 477. **DOI:**10.1016/j.tsf.2004.11.064
3. Sun, R.; Chan, M.; Ceder. G.; *Phys. Rev. B: Condens. Matter Mater. Phys.*,**2011**, 83, 235311 **DOI:**10.1088/0953-8984/25/46/465801
4. Ferrer, I.J.; Sanchez, C.; *J. Appl. Phys.*, **1991**, 70, 2641. **DOI:**org/10.1063/1.349377
5. Soukup, R. J.; Prabukanthan, P.; Ianno, N. J.; Sarkar, A.; Kamler, C. A.; Sekora, D. G.; *J. Vac. Sci. Technol.*, 2011, A 29, 011001. **DOI:** 10.1116/1.3517739
6. Smestad, G.; Ennaoui, A.; Fiechter, S.; Tributsch, H.; Hofmann, W.K.; Birkholz, M.; *Sol. Energy Mater.*, **1990**, 20, 149. **DOI:** 10.1016/0165-1633(90)90001-H
7. Yuan, B.; Luan, W.; Tu, S.T.; *Mater. Lett.*, 2015, 142, 160. **DOI:** 10.1016/j.matlet.2014.12.003
8. Gomes, A.; Mendonc¸aM.H.;. Da Silva Pereira, M.I.; Costa, F.M.A.; *J. Solid State Electrochem.*, **2000**, 4, 168. **DOI:** 10.1007/s100080050015
9. Abass, A. K.; Ahmed, Z. A.; Tahib, R. E.; *Phys. Status Solidi a*,**1986,** 97, 243. **DOI:** 10.1002/pssa.2210970122
10. Smestad, G.; Da Silva, A.; Tributsch, H.; Fiechter, S.; Kunst, M.; Meziani, N.; Birkholz, M.; *Sol. Energy Mater.*, **1989**, 18, 299. **DOI:** 10.1016/0165-1633(89)90044-0
11. Yamamoto, A.; Nakamura, M.; Seki, A.; Li, E. L.; Hashimoto, A.; Nakamura, S; *Sol. Energy Mater. Solar Cells*, **2003**, 75, 451. **DOI:** 10.1016/S0927-0248(02)00205-2
12. Ouertani, B.; Ouerfelli, J.; Saadoun, M.; Bessais, B.; Ezzaouia, H.; Bernede, J. C.; *Mater. Charact.*, **2005**, 54, 431. **DOI:** 10.1016/j.matchar.2005.01.009
13. Yang, K.; Kawai, S.; Ichimura, M.; *Thin Solid Films*, **2014**, 573, 1. **DOI:** 10.1016/j.tsf.2014.10.072
14. Dong, Y.; Zheng, Y.; Duan, H.; Sun, Y.; Chen, Y.; *Mater. Lett.*, **2005**, 59, 2398. **DOI:** 10.1016/j.matlet.2005.03.025
15. Gomes, A.; Ares, J.; Ferrer, I.; Da Silva Pereira, M.; Sanchez, C.; *Mater. Res. Bull.*, **2003**, 38, 1123. **DOI:** 10.1016/S0025-5408(03)00116-8
16. Nakamura, S.; Yamamoto, A.; *Sol. Energy Mater. Sol. Cells*, **2001**, 65, 79. **DOI:** 10.1016/S0927-0248(00)00080-5
17. Chatzitheodorou, G.; Fiechter, S.; Kunst, M.; Luck, J.; Tributsch, H.; *Mater. Res. Bull.*, **1988**, 23, 1261. **DOI:**10.1016/0025-5408(88)90114-6
18. Prabukanthan, P.; Soukup, R. J.; Ianno, N. J.; Sarkar, A.; Kment, S.; Kmentova, H.; Kamler, C. A.; Exstrom, C. L.; Olejnicek, J.; Darveau, S. A.; Proceedings of the 35th Photovoltaics Specialists Conference, Honolulu, HI, United States, June 20-25, 2010, Institute of Electrical and Electronics Engineers: Washington, DC, **2010**; p 2965. **DOI**: 10.1109/PVSC.2010.5614465
19. Duan, H.; Zheng, Y. F.; Dong, Y. Z.; Zhang, X. G.; Sun, Y. F.; *Mater. Res. Bull.*, **2004**, 39, 1861. **DOI:** 10.1016/j.materresbull.2004.06.012
20. Huang, L.; Wang, F.; Luan, Z.; Meng, L.; *Mater. Lett.*, **2010**, 64, 2612. **DOI:** 10.1016/j.matlet.2010.08.070
21. Wang, F.; Huang, L.; Luan, Z.; Huang, J.; Meng, L.; *Mater. Chem. Phys.*, **2012**, 132, 505. **DOI:** 10.1016/j.matchemphys.2011.11.061
22. Zhu, L.; Richardson, B.; Tanumihardja, J.; Yu, Q.; *Cryst. Eng. Comm*, **2012**, 14, 4188. **DOI:** 10.1039/C2CE25222H
23. Kirkeminde,K.; Scott, R.; Ren,S.; *Nanoscale*, **2012**, 4, 7649. **DOI:** 10.1039/c2nr32097e
24. Vaughan, D.J.; Craig, J.R.; Mireral Chemistry of Metal Sulfides, Cambridge University Press, Cambridge, U.K. **1978**
25. Ferrer, I.J.; Sanchez, C.; *Solid State Commun.***1992**, 81, 317 **DOI:** 10.1016/0038-1098(92)90759-3
26. Schroder, D.K.; Semiconductor Material and Device Characterization, Chapter 1.10, 30th Edition, John Wiley & Sons, New Jersey **2006**.

